ADVANCES IN ATMOSPHERIC SCIENCES, VOL. 29, NO. 6, 2012, 1174–1184

The Behaviors of Optimal Precursors during Wintertime Eurasian Blocking Onset

JIANG Zhina* (姜智娜) and WANG Donghai (王东海)

State Key Laboratory of Severe Weather, Chinese Academy of Meteorological Sciences, Beijing 100081

(Received 8 July 2011; revised 6 February 2012)

ABSTRACT

In this paper the optimal precursors for wintertime Eurasian blocking onset are acquired by solving a nonlinear optimization problem whose objective function is constructed based on a blocking index with a triangular T21, three-level, quasi-geostrophic global spectral model. The winter climatological state is chosen as the reference basic state. Numerical results show that the optimal precursors are characterized by a baroclinic pattern with a westward tilt with height, which are mainly located upstream of the blocking region. For an optimization time of 5 days, these perturbations are mainly localized over the Northeast Atlantic Ocean and continental Europe. With the extension of the optimization time to 8 days, these perturbations are distributed more upstream and extensively in the zonal direction. Wave spectrum analysis reveals that the optimal precursors are composed of not only synoptic-scale (wave numbers 5–18) waves, but planetary-scale (wave numbers 0–4) waves as well. The synoptic-scale optimal precursors are mainly located in the mid-latitude area, while the planetary-scale optimal precursors focus primarily on the high-latitude region. The formation of a strong planetary-scale positive blocking anomaly is accompanied by the reinforcement of synoptic-scale perturbations and further fragmentation into two branches, in which the northern branch is generally stronger than the southern one. The eddy forcing arising from the self-interaction of synoptic-scale disturbances is shown to be crucial in triggering the dipole blocking anomaly, and the planetary-scale optimal precursor provides the initial favorable background conditions for blocking onset.

Key words: nonlinear optimization problem, wave spectrum analysis, self-interaction

Citation: Jiang, Z. N., and D. H. Wang, 2012: The behaviors of optimal precursors during wintertime Eurasian blocking onset. *Adv. Atmos. Sci.*, **29**(6), 1174–1184, doi: 10.1007/s00376-012-1102-3.

1. Introduction

Atmospheric blocking has long been recognized to have a profound impact on weather and climate, inducing extremely high or low temperatures and severe precipitation over its surrounding areas (Rex, 1950a, b; Wang et al., 2009). However, weather forecasts during blocking onset still frequently suffer from a rapid loss of predictability (Frederiksen et al., 2005). Therefore, it is important to capture the precursors to blocking onset and understand its mechanism of development, so as to provide a better weather forecast.

Many observational studies have been devoted to exploring the factors related to blocking onset, such as background flow, planetary-scale and synoptic-scale waves and external forcing (Berggren et al., 1949; Colucci, 1985, 1987; Nakamura and Wallace, 1993; Liu et al., 1996; Nakamura et al., 1997; Michelangeli and Vautard, 1998; Colucci, 2001; Dong and Colucci, 2005; Han et al., 2011). Theoretical work has also been carried out. Frederiksen (1998) explored the precursors to the Pacific–North American and North Atlantic blockings with an explicit matrix inversion using a two-level tangent linear model with time-dependent basic states taken from observations. The results showed that the precursors are upstream of the blockings. Li et al. (1999) described the dynamics of adjoint sensitivity perturbations that excite block onsets over the Pacific and Atlantic Oceans using a hemispherical, primitive equations, θ-coordinate, two-layer model. The results showed that for both the Pacific and Atlantic blockings, sensitivity perturbations expressed in terms of vertical vorticity displayed a Rossby wave train structure mainly found on the southward flanks of the Pa-

*Corresponding author: JIANG Zhina, jzn@cams.cma.gov.cn

cific and Atlantic jets. Li et al. (2001) identified the location and structure of optimal perturbations favorable for the development and maintenance of the Ural blocking in the rainy season using the adjoint method. The authors showed that the growth of the ridge over the Ural Mountains tends to organize transient eddies into the region upstream from the central North Atlantic to coastal Western Europe. The study also demonstrated that the optimal sensitivity perturbation approach is based on a linear framework, which may not be applicable in an episode of long duration. Luo et al. (2001) and Luo (2005) examined the interaction between antecedent planetary-scale envelope solution blocking anticyclones and synoptic-scale eddies, pointing out that both the antecedent synoptic-scale eddies that induce a low/high eddy forcing pattern, and the weak background westerly flow that allows a quasi-stationary preblock ridge to form, are two necessary preconditions for the onset of a blocking anticyclone. Jiang and Wang (2010) explored the precursors to blocking anomalies over two oceans in climatological flows by using the theory of conditional nonlinear optimal perturbations. They pointed out that the precursors are baroclinic wave train disturbances, which mainly focus on the northward flanks of the corresponding Atlantic and Pacific upper-level jets, taking on a northeast–southwest trend.

The present study was motivated by Luo et al. (2001) and Luo (2005). We extend the work reported by Jiang and Wang (2010) and explore the planetary and synoptic-scale behaviors of the optimal precursors for the Eurasian blocking onset in the winter season. Based on this, we further investigate the interaction of the planetary- and synoptic-scale waves, and hope to capture the main dynamical process dominating the blocking onset.

The outline of the paper is as follows. In section 2, we summarize the model and present the corresponding nonlinear optimization problem. Section 3 presents the numerical results, and a zonal harmonic decomposition is performed on the optimal precursors. Conclusions are summarized in section 4.

2. Preparation: model and method

2.1 *Model and the definition of blocking*

A triangular truncation T21L3 (three layers: 200 hPa, 500 hPa and 800 hPa), quasi-geostrophic global spectral model was used for this study. This was chosen because it is simple, but also able to generate a very realistic winter climatology in a long nonlinear integration. Furthermore, two regimes (blocking and strong zonal flow), similar to those observed (Marshall and Molteni, 1993) could be modeled.

There are many criteria for identifying a blocking flow (Lejenäs and Økland, 1983; Tibaldi and Molteni, 1990; Lupo and Smith, 1995; Pelly and Hoskins, 2003; Diao et al., 2006). Here, the blocking index B, introduced by Liu (1994), is adopted to measure the resemblance of a particular circulation pattern to the blocking regime, an approach that has been successfully used in many sensitivity analysis and predictability studies (Oortwijn and Barkmeijer, 1995; Oortwijn, 1998; Li et al., 1999).

$$B = \frac{< \boldsymbol{\psi}_{\rm b}, \boldsymbol{\psi}_{\rm d} >}{< \boldsymbol{\psi}_{\rm b}, \boldsymbol{\psi}_{\rm b} >} , \tag{1}$$

where $\boldsymbol{\psi}_{\rm b}$ ($\boldsymbol{\psi}_{\rm d}$) is the specified stream function blocking anomaly (daily stream function anomaly) over the climatological mean. The angle brackets denote the Euclidean inner product on a sphere, integrated over height

$$\langle \boldsymbol{x}, \boldsymbol{y} \rangle = \iiint \boldsymbol{x}\boldsymbol{y} dV , \tag{2}$$

where V represents the integration over the whole atmosphere. A circulation pattern with B larger than some threshold is defined as a blocking flow. Note that a larger positive B corresponds to a more pronounced blocking flow.

2.2 *Description of the nonlinear optimization problem*

To obtain the optimal precursor triggering blocking onset, we first construct a nonlinear optimization problem related to it, similar to the approach used by Jiang and Wang (2010). The winter climatological flow is chosen as a reference trajectory, and the objective function is constructed according to the above blocking index. The difference is that here we investigate a Eurasian blocking weather event. Therefore, the Atlantic blocking anomaly pattern obtained in Jiang and Wang (2010) is shifted to the Eurasian continent from about 45°E to 135°E, which can be referred to in Oortwijn (1998) and Li et al. (1999).

As in Jiang and Wang (2010) the nonlinear optimization problem in the present study has been illustrated clearly, and can be simplified as follows. Assuming the dynamical system equations of T21L3 and the initial state $\boldsymbol{Q}_0$ are known exactly, the future state at time T can be written as

$$\boldsymbol{Q}(T) = \boldsymbol{M}_{\rm T}(\boldsymbol{Q}_0) , \tag{3}$$

where $\boldsymbol{Q}$ denotes the column vector of quasi-geostropic potential vorticity spectral coefficients, and $\boldsymbol{M}_{\rm T}$ represents the nonlinear propagator of the T21L3 model equation.

The optimal precursor that triggers the blocking onset is the initial perturbation $\boldsymbol{q}_0^*$, which satisfies the initial constraint condition $\|\boldsymbol{q}_0^*\| \leqslant \sigma$ and causes the

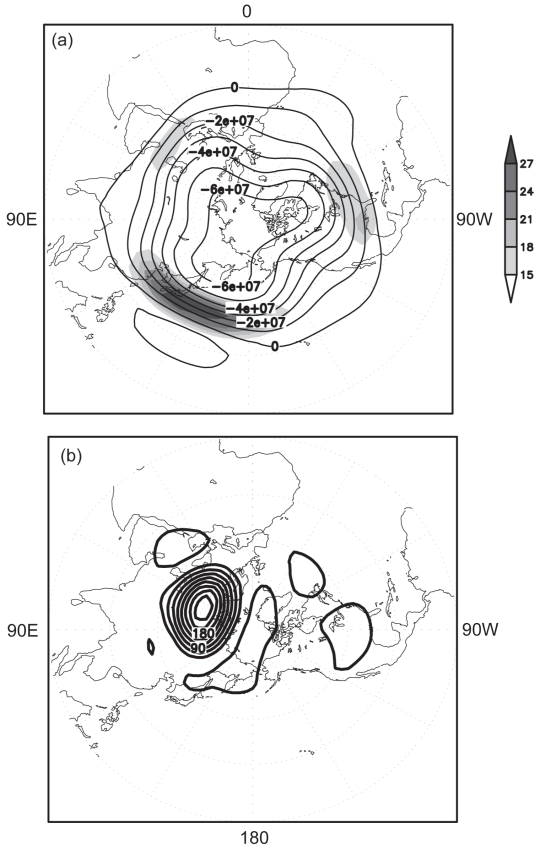

Fig. 1. (a) The 500-hPa stream function ($m^2\ s^{-1}$; contours) and zonal wind ($m\ s^{-1}$; shaded) of the climatological flow. (b) The blocking anomaly over the Eurasian continent (gpm).

objective function $J(\boldsymbol{q}_0)$ to achieve the maximum value. Here, we define

$$J(\boldsymbol{q}_0^*) = \max_{\|\boldsymbol{q}_0\| \leqslant \sigma} J(\boldsymbol{q}_0)\ , \tag{4}$$

and

$$J(\boldsymbol{q}_0) = \frac{< \boldsymbol{F}[\boldsymbol{M}_{\rm T}(\boldsymbol{Q}_0 + \boldsymbol{q}_0)] - \boldsymbol{\psi}_{\rm c},\ \boldsymbol{\psi}_{\rm b} >}{< \boldsymbol{\psi}_{\rm b}, \boldsymbol{\psi}_{\rm b} >}\ , \tag{5}$$

where $\psi_{\rm c}$ is the steam function climatological flow. $\boldsymbol{F}$ is an operator that transforms the potential vorticity of the basic state to the stream function field, $\boldsymbol{Q}_0$ is the initial potential vorticity field of reference state, and $\boldsymbol{q}_0$ is a randomly assigned initial potential vorticity perturbation that satisfies $\|\boldsymbol{q}_0\| \leqslant \sigma$. A presumed positive constant σ represents an upper-bound of the initial perturbation magnitude.

The above nonlinear optimization problem can be solved numerically. The optimization algorithm known as "spectral projected gradient 2" (SPG2) (Birgin et al., 2000) is employed, which can calculate the least value of a function subject to initial constraint conditions. Then, the above constructed objective function is transformed to another new objective function, which is the negative of the original objective function.

Similarly, the linear optimal precursor is obtained by maximizing a modified version of the objective function, which is acquired by replacing the nonlinear

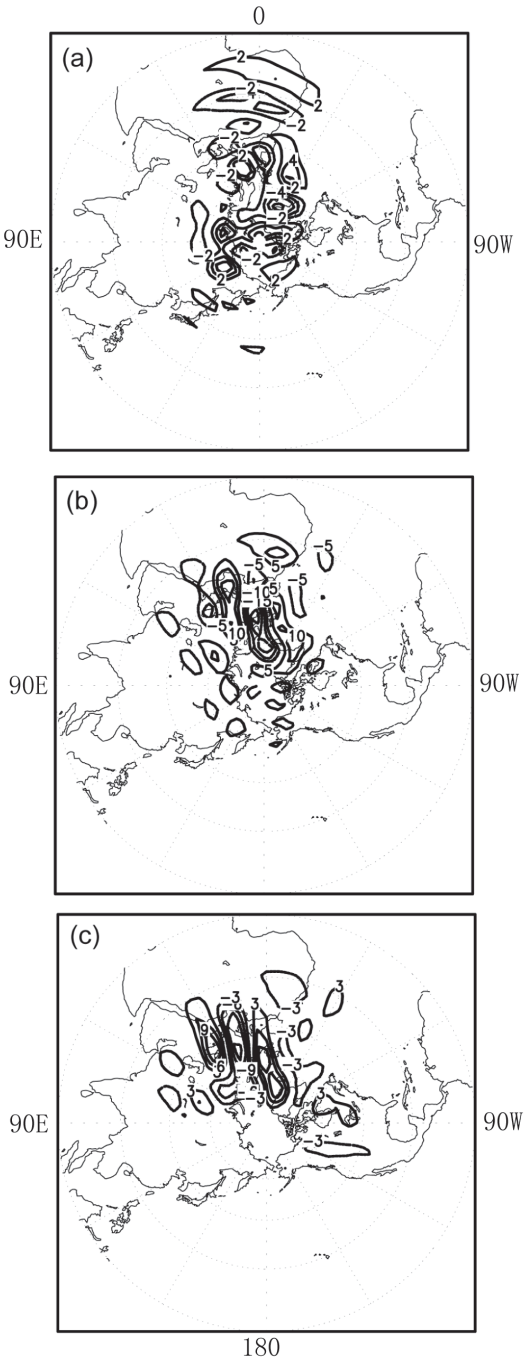

Fig. 2. The optimal precursor (gpm) triggering the blocking onset for an optimization time of 5 days at three levels: (a) at 200 hPa; (b) at 500 hPa; (c) at 800 hPa.

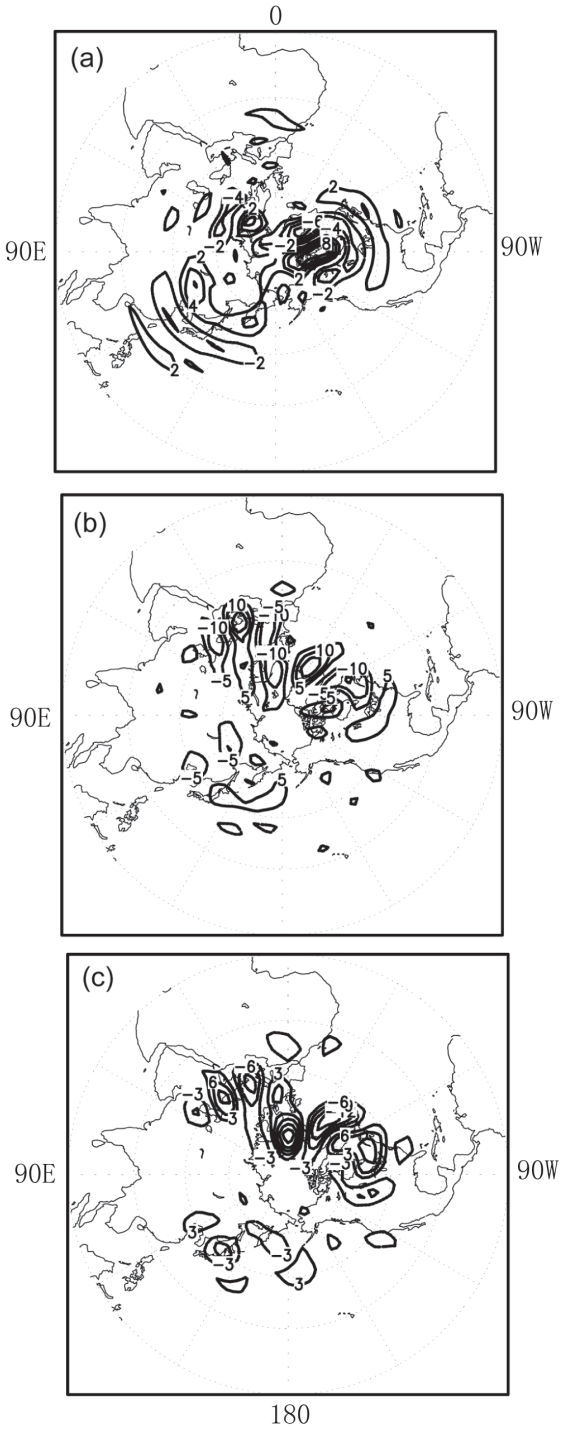

Fig. 3. Same as Fig. 2, but for an optimization time of 8 days.

evolution of the reference initial basic state plus the initial perturbation with the nonlinear evolution of the reference initial basic state plus the tangent linear evolution of the initial perturbation, which can be referred to Mu and Jiang (2008).

3. Numerical experiments

In the following numerical experiments, the initial constraint condition $\sigma = 4.0\times10^5$ m^2 s^{-1} is chosen, so that the amplitude of initial geopotential height perturbation at 500 hPa is within 20 geopotential meters (gpm). The optimal precursors are computed with an optimization time interval of 5 and 8 days, respectively. Figure 1a shows the 500-hPa stream function and zonal wind of the climatological flow, which is constructed from an 1800-day (corresponding to 20 winters) integration using the T21L3 quasi-geostrophic model with the initial conditions of the European Centre for Medium-Range Weather Forecast's analysis of 0000 UTC 1 December 1983. The simulated winter climatological flow is identical to the observed, with three low troughs and three high ridges. The Eurasian blocking anomaly pattern is shown in Fig. 1b, which has a strong positive anomaly lying over the Ural Mountains.

3.1 *Optimal precursors to blocking onset*

Figure 2 presents the optimal precursors for an optimization time of 5 days at three levels. It is clear that these perturbations are characterized by a baroclinic pattern with a westward tilt with height. In addition, in the zonal direction these perturbations show localization, being mainly located over the Northeast Atlantic Ocean and continental Europe. In the meridional direction, the localization characteristics of these perturbations are strongest at 800 hPa, mainly focused on the mid-latitude region. At 500 hPa, they extend northward to high-latitude areas, and at 200 hPa they are distributed from high to mid latitudes and even into the tropics.

If we extend the optimization time, what characteristics will these perturbations exhibit? Figure 3 presents the optimal precursors for an optimization time of 8 days at three levels. It can be seen that these baroclinic wave trains are located more upstream than those with an optimization time of 5 days. Moreover, localization for these perturbations becomes weak, being found not only over the whole of the northern Atlantic Ocean and continental Europe, but also over the East Asian continent and the Northwest Pacific Ocean.

Linear optimal precursors with an optimization time of 5 and 8 days at 500 hPa are shown in Fig. 4. It can be seen that the linear optimal precursors are also wave trains located upstream of the blocking region; however, there are great differences between them and the optimal precursors with the same optimization time. That is to say, the linear approximation has some limitations when the optimization time is not too short.

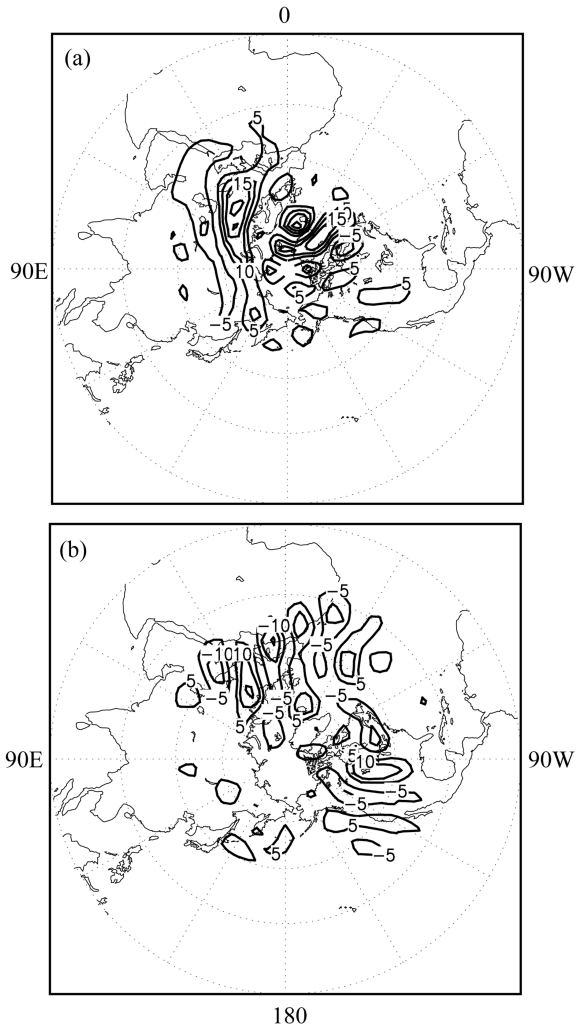

Fig. 4. The linear optimal precursor (gpm) triggering the blocking onset at 500 hPa for an optimization time of (a) 5 days; (b) 8 days.

3.2 *Wave spectrum analysis*

In order to see the dominant modes of optimal precursors, we perform a zonal harmonic decomposition, shown in Fig. 5. It is clear that the optimal precursors are composed of not only synoptic-scale (wave numbers 5–18) waves, but also planetary-scale (wave numbers 0–4) waves. However, wave numbers 5 and 6 may be the dominant modes for the initial optimal precursors. This finding is different from that of Frederiksen (1998) and Li et al. (1999), who reported that the sensitivity perturbations are smaller-scale wave train and Rossby wave train structures, respectively.

According to the definition of Rex (1950a), the width of blocking must extend over at least 45° of longitude, which corresponds to wave number 4 in the zonal direction. Therefore, the evolution of the blocking anomaly can be clearly revealed from the planetary-scale part of the nonlinear evolution of the optimal precursors. Figure 6 presents the nonlinear evolution of the optimal precursor and its respective planetary- and synoptic-scale parts at 500 hPa for an optimization time of 5 days. It can be seen that the synoptic-scale optimal precursors are mainly located in the mid-latitude area, while the planetary-scale optimal precursors focus primarily on the high-latitude region. With time, the planetary-scale parts amplify from the high- to mid-latitude area. At the optimization time, a very strong positive anomaly around the Ural Mountains forms, and three negative anomalies accompany it in its western, southern and eastern directions, respectively. Meanwhile, the synoptic-scale parts propagate downstream and amplify with time. At the final time, the wave trains are distributed almost entirely in the zonal direction, except over the North American continent. The nonlinear evolution of the optimal precursor and its respective planetary- and synoptic-scale parts at 500 hPa for an optimization time of 8 days are shown in Fig. 7. The evident differences are that the planetary-scale positive anomaly over the Ural Mountains becomes stronger and the synoptic-scale waves divide into two branches over the blocking region with time, in which the northern branch is generally stronger than the southern one.

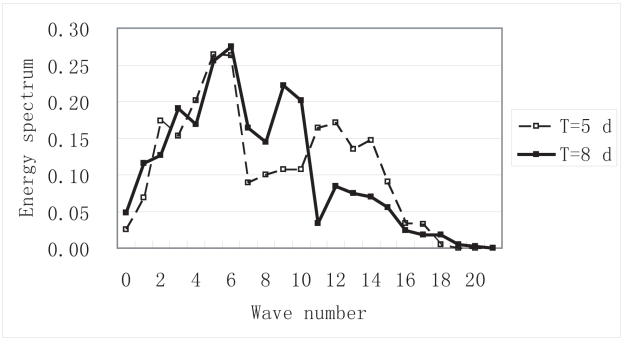

Fig. 5. The energy spectrum of the optimal precursor (J kg^{-1}) as a function of the total wave number for the optimization time of 5 and 8 days.

To see the effect of the optimal precursor on the basic state, we present the perturbed stream function field at the optimization time at 500 hPa in Fig. 8. It can be seen that for an optimization time of 5 days, only a strong meridional flow over the Eurasian continent forms, and for an optimization time of 8 days we may observe a Eurasian blocking high. In conclusion, the planetary-scale optimal precursor may provide the favorable background conditions for the formation of a strong meridional flow and/or a blocking high, whose development meanwhile accompanies the reinforcement and furthermore division into two branches of synoptic-scale perturbations.

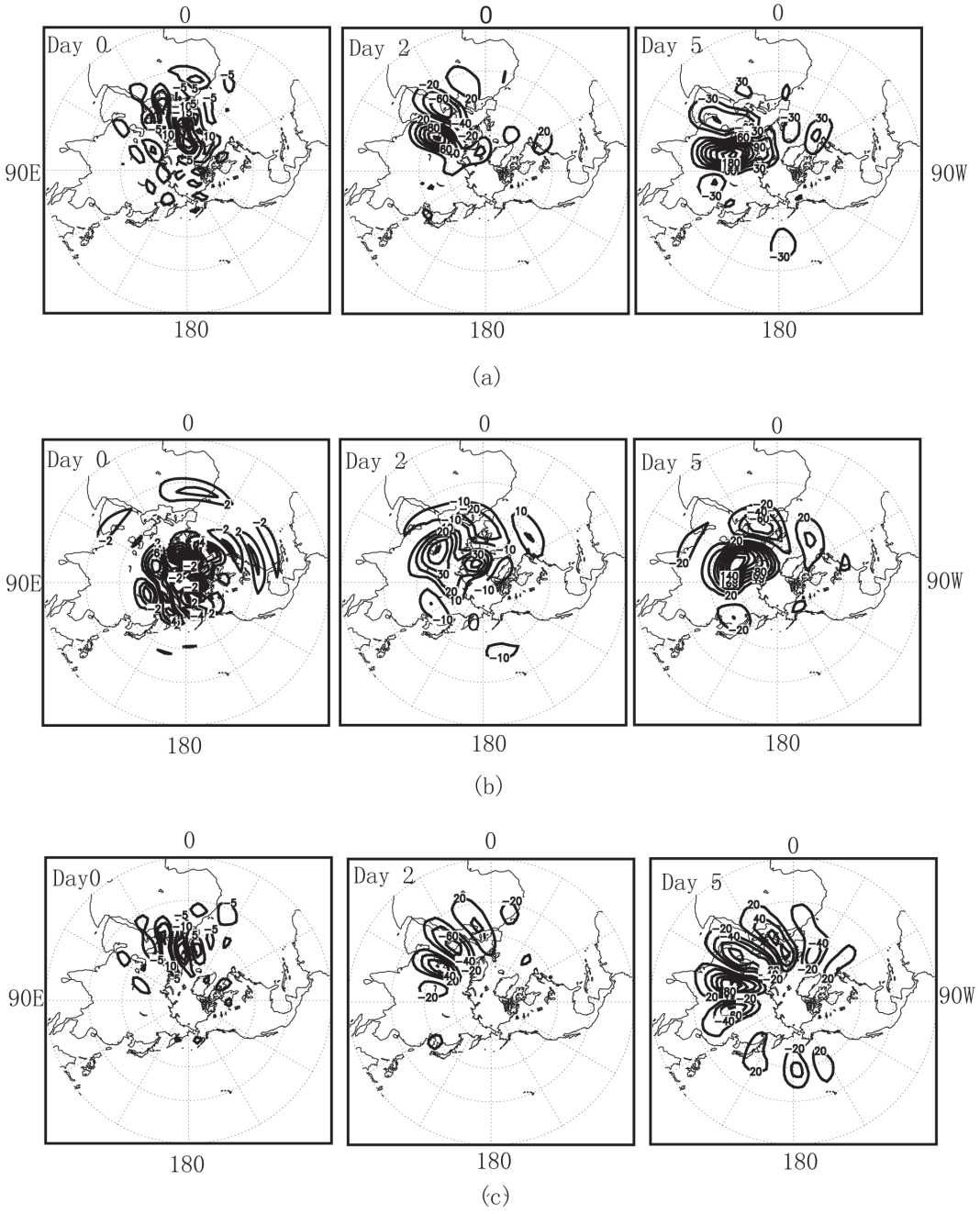

Fig. 6. The nonlinear evolution of the optimal precursor and its respective planetary- and synoptic-scale parts at 500 hPa for an optimization time of 5 days: (a) the perturbation; (b) the planetary-scale part; (c) the synoptic-scale part.

3.3 *On the interpretation of blocking onset*

From the above subsection, we know that the optimal precursors consist of two parts: a planetary-scale and a synoptic-scale part. What are the contributions of these two parts to blocking onset? How do the initial optimal precursors develop into a positive anomaly over the Ural Mountains? In this subsection, we try to provide an explanation from the potential vorticity point of view. Firstly, the streamfunction is decomposed as

$$\psi_i = \bar{\psi}_i + \psi'_i \,,$$

where $\bar{\psi}_i$ is the reference basic state, and ψ'_i is the perturbation. Thus, the perturbation evolution equation

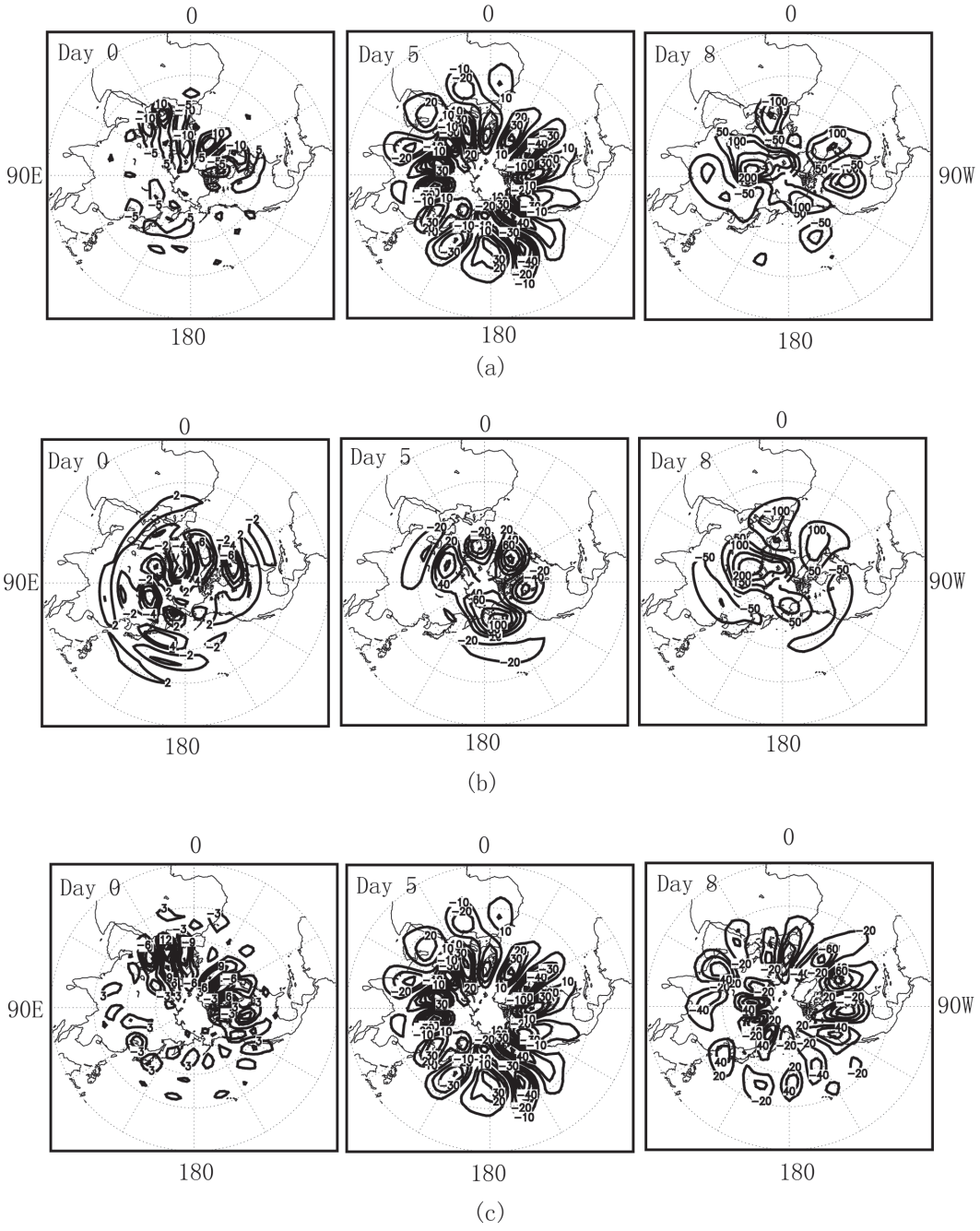

Fig. 7. Same as Fig. 6, but for an optimization time of 8 days.

is

$$\frac{\partial q_i'}{\partial t} = -J(\bar{\psi}_i, q_i') - J(\psi_i', \bar{Q}_i) - J(\psi_i', q_i') - D_i' \,, \quad (6)$$

where $i = 1, 2, 3$ represents three levels, and $\bar{Q}_i(q_i')$ is the potential vorticity of the reference basic state (the perturbation).

Furthermore, the perturbation $\psi_i'(q_i')$ contains two parts: time-dependent planetary-scale disturbances $\psi_{ip}'(q_{ip}')$ (wave numbers 0–4) and synoptic-scale disturbances $\psi_{is}'(q_{is}')$ (wave numbers 5–16). Then, the decompositions

$$\psi_i' = \psi_{ip}' + \psi_{is}' \,,$$

and

$$q_i' = q_{ip}' + q_{is}' \,,$$

can be made according to Luo (2005), allowing us to obtain

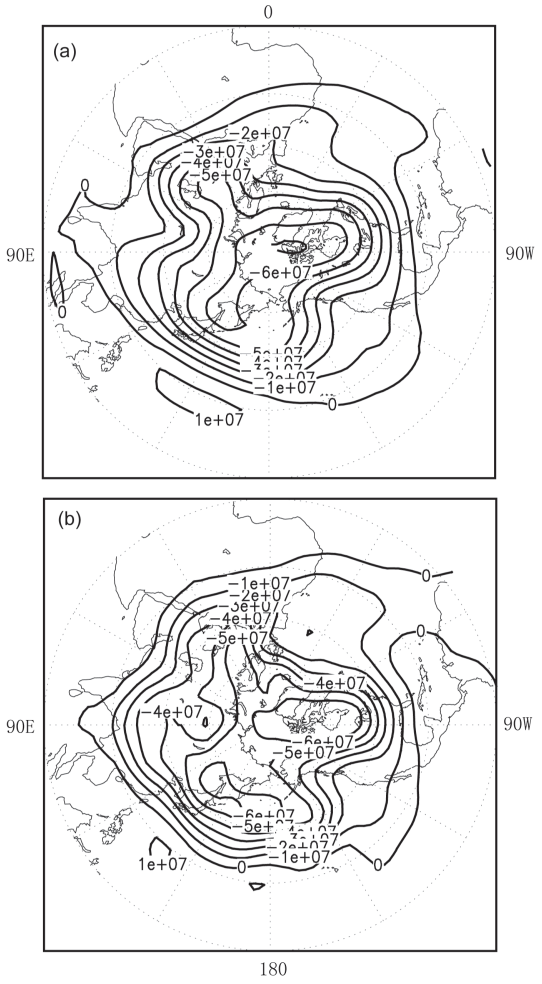

Fig. 8. The perturbed streamfunction field (m^2 s^{-1}) at the optimization time at 500 hPa: (a) for an optimization time of 5 days; (b) for an optimization time of 8 days.

$$\frac{\partial q'_i}{\partial t} = -J(\bar{\psi}_i, q'_{ip} + q'_{is}) - J(\psi'_{ip} + \psi'_{is}, \bar{Q}_i) - J(\psi'_{is}, q'_{ip}) - J(\psi'_{ip}, q'_{is}) - J(\psi'_{ip}, q'_{ip}) - J(\psi'_{is}, q'_{is}) - D'_i \,. \tag{7}$$

It is obvious that the evolution of perturbation is dominated by interaction of the disturbances and the basic state [the first two terms on the right hand side of Eq. (7)], interaction of the planetary-scale and synoptic-scale disturbances [the third and fourth terms on the right hand side of Eq. (7)], self-interaction of planetary-scale disturbances [the fifth term on the right hand side of Eq. (7)], self-interaction of synoptic-scale disturbances [the sixth term on the right hand side of Eq. (7)], and the dissipation D'_i. Because the dissipation term always displays an anomaly pattern that is opposite to the anomaly of the potential vorticity, we focus on the advection terms, which have more interesting behaviors. To observe the effect of potential vorticity advection on planetary-scale perturbation evolution, we calculate the time mean planetary-scale (wave numbers 0–4) projections of the above potential vorticity advection terms for an optimization time of 5 and 8 days, the results of which are shown in Figs. 9 and 10, respectively. Comparatively, it is evident that the self-interaction of synoptic-scale disturbances presents a low/high pattern between 20°N and 70°N over the blocking region and is upstream for the optimization time of both 5 and 8 days, as shown in Figs. 9d and 10d, respectively. The negative (or positive) value region over north (or south) of 40°N represents anticyclonic (or cyclonic) vorticity advection, which means that the anticyclonic (or cyclonic) vorticities induced by self-interaction of synoptic-scale disturbances are injected into the high (or low) pressure blocking region. The vorticity then promotes the development of the anticyclone (low pressure) of the dipole blocking anomaly. Furthermore, for the optimization time of 5 days, though the patterns between 20°N and 70°N induced by interaction of the planetary- and synoptic-scale disturbances, and self-interaction of the planetary-scale disturbances, exhibit low/high structures over the Ural Mountains, they are weak whether in terms of strength or spatial size (shown in Figs. 9b and c). Moreover, the potential vorticity transport induced by interaction of the disturbances and the basic state exhibits a strong negative anomaly around 40°N over the blocking region (Fig. 9a). The effect of this on blocking onset is complex. However, for the optimization time of 8 days, the potential vorticity transport induced by the interaction of the planetary- and synoptic-scale disturbances around 90°E presents a strong positive anomaly along 45°N, which may play a negative role in blocking onset (Fig. 10b). Furthermore, the potential vorticity transport induced by self-interaction of the planetary-scale perturbation mainly focuses on the high-latitude areas, exhibiting cyclonic vorticity advection north of 40°N around 90°E, thus prohibiting the evolution of the positive blocking anomaly (Fig. 10c). Similarly, the potential vorticity transport induced by interaction of the disturbances and the basic state is also complex, exhibiting cyclonic (or anticyclonic) vorticity advection east (or west) of 90°E north of 40°N (Fig. 10a). In conclusion, the self-interaction of the synoptic-scale parts of optimal precursors indeed plays a primary role in triggering the onset of blocking.

4. Conclusions

In this paper, we have explored the optimal precursors for Eurasian blocking onset in winter by numerically solving a nonlinear optimization problem, which

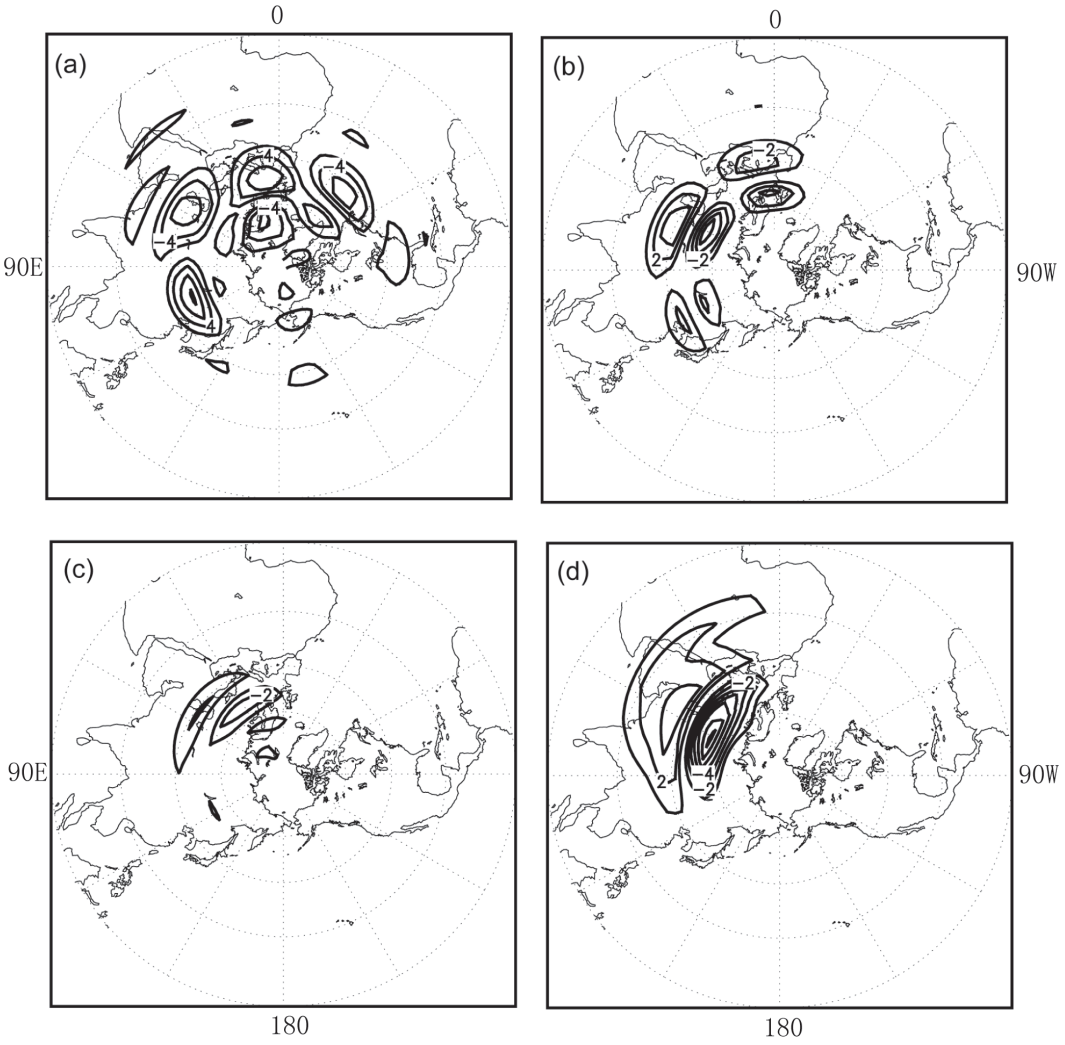

Fig. 9. The time mean planetary-scale projection of vorticity transport (in 10^{-11} s^{-2}) for an optimization time of 5 days: (a) interaction of the disturbances and the basic state; (b) interaction of the planetary- and synoptic-scale disturbances; (c) self-interaction of the planetary-scale perturbation; (d) self-interaction of synoptic-scale disturbances.

was constructed according to a blocking index. The winter climatological flow was chosen as a reference trajectory, and the results for an optimization time of 5 and 8 days have been presented.

The results showed that there were great differences between the optimal precursor and its linear counterpart, illustrating that linear approximation has some limitations. The optimal precursor was composed of not only planetary-scale (wave numbers 0–4) waves, but synoptic-scale (wave numbers 5–18) waves as well, which were characterized by a baroclinic pattern with a westward tilt with height. The synoptic-scale optimal precursors were mainly located in the mid-latitude area, while the planetary-scale optimal precursors mainly focused on the high-latitude region. For an optimization time of 5 days, these perturbations were mainly located over the Northeast Atlantic Ocean and continental Europe. With time, a planetary-scale positive anomaly formed over the Ural Mountains, accompanied by the propagation and amplification of the synoptic-scale wave trains over this area. At the optimization time, a strong meridional flow could be observed. When the optimization time was extended to 8 days, the optimal precursors were found to be more upstream and their tendency to be localized became very weak. With time, a stronger planetary-scale positive anomaly formed over the Ural Mountains, and the synoptic-scale wave trains amplified and then divided into two branches over this area, in which the northern branch was generally stronger than the southern one. For this case, one could see a blocking high forming.

We may conclude that the formation of a strong

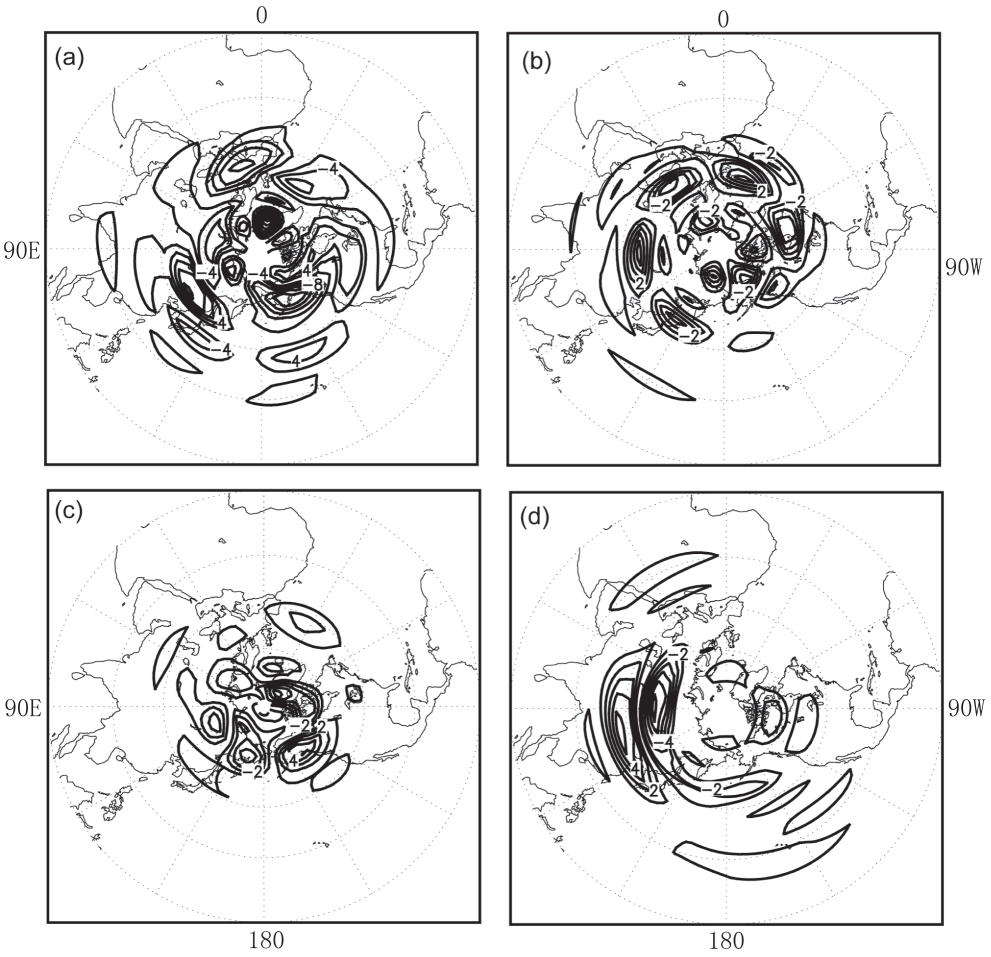

Fig. 10. Same as Fig. 9, but for an optimization time of 8 days.

meridional flow is accompanied by the reinforcement of synoptic-scale waves, and the formation of a blocking high is accompanied by the division in north-south direction of synoptic-scale waves over the blocking region. Jiang and Wang (2010) pointed out that self-interaction of the disturbances plays an important role in triggering the blocking onset. In this research, by further calculating the potential vorticity transport of the planetary- and synoptic-scale wave parts, we have found that the self-interaction of the synoptic-scale wave part in the self-interaction of the disturbances is the most fundamental in triggering the strong meridional flow and even the blocking onset, which is consistent with Luo et al. (2001) and Luo (2005).

Acknowledgements. This research was motivated by insightful discussion with Prof. LUO Dehai. It was supported by the National Natural Science Foundation of China (Grant No. 40905023) and the National Key Basic Research and Development (973) Project (Grant No. 2012CB417200). The authors are grateful to the two anonymous reviewers for their valuable comments and suggestions.

REFERENCES

Berggren, R., B. Bolin, and C. G. Rossby, 1949: An aero logical study of zonal motion, its perturbation and break-down. *Tellus,* **1**, 14–37.

Birgin, E. G., J. M. Martinez, and M. Raydan, 2000: Nonmonotone spectral projected gradient methods for convex sets. *Society for Industrial and Applied Mathematics Journal on Optimization*, **10**(4), 1196–1211.

Colucci, S. J., 1985: Explosive cyclogenesis and large-scale circulation changes: Implications for atmospheric blocking. *J. Atmos. Sci.*, **42**, 2710–2717.

Colucci, S. J., 1987: Comparative diagnosis of blocking versus nonblocking planetary-scale circulation changes during synoptic-scale cyclogenesis. *J. Atmos. Sci.*, **44**, 124–139.

Colucci, S. J., 2001: Planetary-scale preconditioning for the onset of blocking. *J. Atmos. Sci.*, **58**, 933–942.

Diao, Y. N., J. P. Li, and D. H. Luo, 2006: A new block-

ing index and its application: Blocking action in the northern hemisphere. *J. Climate,* **19**, 4819–4839.

Dong, L., and S. J. Colucci, 2005: The role of deformation and potential vorticity in southern hemisphere blocking onsets. *J. Atmos. Sci.*, **62**, 4043–4056.

Frederiksen, J. S., 1998: Precursors to blocking anomalies: The tangent linear and inverse problems. *J. Atmos. Sci.*, **55**, 2419–2436.

Frederiksen, J. S., M. A. Collier, and A. B. Watkins, 2005: Dependence of ensemble prediction skill on blocking instability regimes. *Tellus*, **56A**, 485–500.

Han, Z., S. L. Li, and M. Mu, 2011: The role of warm north Atlantic SST in the formation of positive height anomalies over the Ural Mountain during January 2008. *Adv. Atmos. Sci.*, **28**(2), 246–256, doi: 10.1007/s00376-010-0069-1.

Jiang, Z. N., and D. H. Wang, 2010: A study on precursors to blocking anomalies in climatological flows by using conditional nonlinear optimal perturbations. *Quart. J. Roy. Meteor. Soc.*, **136**(650), 1170–1180.

Lejenäs, H., and H. Økland, 1983: Characteristics of northern hemisphere blocking as determined from a long time series of observational data. *Tellus,* **35A**, 350–362.

Li, S. L., L. R. Ji, and W. T. Lin, 2001: On the formation and maintenance of the persistent anomalies of summertime circulation over the Ural Mountains. *Adv. Atmos. Sci.*, **18**(5), 819–830.

Li, Z. J., A. Barcilon, and I. M. Navon, 1999: Study of block onset using sensitivity perturbations in climatological flows. *Mon. Wea. Rev.*, **127**, 879–900.

Liu, H., G. X. Wu, and Q. C. Zeng, 1996: On the maintenance of blocking anticyclones of Northern Hemisphere. Part I: Quasi-geostrophic potential vorticity analysis. *Acta Meteorologica Sinica*, **10**(2), 142–147. (in Chinese)

Liu, Q., 1994: On the definition and persistence of blocking. *Tellus*, **46A**, 286–298.

Luo, D. H., 2005: A barotropic envelope Rossby solution model for block-eddy interaction. Part I: Effect of topography. *J. Atmos. Sci.*, **62**, 5–21.

Luo, D. H., F. Huang, and Y. N. Diao, 2001: Interaction between antecedent planetary-scale envelope soliton blocking anticyclone and synoptic-scale eddies: Observations and theory. *J. Geophys. Res.*, **106**(D23), 31795–31815.

Lupo, A. R., and P. J. Smith, 1995: Climatological features of blocking anticyclones in the northern hemisphere. *Tellus,* **47A**, 439–456.

Marshall, J., and F. Molteni, 1993: Toward a dynamical understanding of planetary- scale flow regimes. *J. Atmos. Sci.*, **50**, 1792–1818.

Michelangeli, P. A., and R. Vautard, 1998: The dynamics of Euro-Atlantic blocking onsets. *Quart. J. Roy. Meteor. Soc.*, **124**, 1045–1070. doi: 10.1002/qj.49712454803.

Mu, M., and Z. N. Jiang, 2008: A method to find perturbations that trigger blocking onset: conditional nonlinear optimal perturbations. *J. Atmos. Sci.*, **65**, 3935–3946.

Nakamura, H., and J. M. Wallace, 1993: Synoptic behavior of baroclinic eddies during the blocking onset. *J. Atmos. Sci.*, **121**, 1892–1903.

Nakamura, H., M. Nakamura, J. L. Anderson, 1997: The role of high- and low-frequency dynamics in blocking formation. *Mon. Wea. Rev.*, **125**(9), 2074–2093.

Oortwijn, J., 1998: Predictability of the onset of blocking an strong zonal flow regimes. *J. Atmos. Sci.*, **55**, 973–994.

Oortwijn, J., and J. Barkmeijer, 1995: Perturbations that optimally trigger weather regime. *J. Atmos. Sci.*, **52**(22), 3932–3944.

Pelly, J. L., and B. J. Hoskins, 2003: A new perspective on blocking. *J. Atmos. Sci.,* **60**, 743–755.

Rex, D. F., 1950a: Blocking action in the middle troposphere and its effects upon regional climate. I: An aerological study of blocking action. *Tellus*, **2**, 196–211.

Rex, D. F., 1950b: Blocking action in the middle troposphere and its effects upon regional climate. II: The climatology of blocking action. *Tellus*, **2**, 275–301.

Tibaldi, S., and F. Molteni, 1990: On the operational predictability of blocking. *Tellus*, **42A**, 343–365.

Wang, D. H., and Coauthors, 2009: A preliminary analysis of features and causes of the snow storm event over the southern areas of China in January 2008. *Acta Meteorological Sinica*, **23**(3), 374–386. (in Chinese)